Precise measurement of hadronic τ-decays in modes with η mesons

K. Abe,[10] I. Adachi,[10] H. Aihara,[52] K. Arinstein,[1] T. Aso,[56] V. Aulchenko,[1] T. Aushev,[22,16] T. Aziz,[48] S. Bahinipati,[3] A. M. Bakich,[47] V. Balagura,[16] Y. Ban,[38] S. Banerjee,[48] E. Barberio,[25] A. Bay,[22] I. Bedny,[1] K. Belous,[15] V. Bhardwaj,[37] U. Bitenc,[17] S. Blyth,[29] A. Bondar,[1] A. Bozek,[31] M. Bračko,[24,17] J. Brodzicka,[10] T. E. Browder,[9] M.-C. Chang,[4] P. Chang,[30] Y. Chao,[30] A. Chen,[28] K.-F. Chen,[30] W. T. Chen,[28] B. G. Cheon,[8] C.-C. Chiang,[30] R. Chistov,[16] I.-S. Cho,[58] S.-K. Choi,[7] Y. Choi,[46] Y. K. Choi,[46] S. Cole,[47] J. Dalseno,[25] M. Danilov,[16] A. Das,[48] M. Dash,[57] J. Dragic,[10] A. Drutskoy,[3] S. Eidelman,[1] D. Epifanov,[1] S. Fratina,[17] H. Fujii,[10] M. Fujikawa,[27] N. Gabyshev,[1] A. Garmash,[40] A. Go,[28] G. Gokhroo,[48] P. Goldenzweig,[3] B. Golob,[23,17] M. Grosse Perdekamp,[12,41] H. Guler,[9] H. Ha,[19] J. Haba,[10] K. Hara,[26] T. Hara,[36] Y. Hasegawa,[45] N. C. Hastings,[52] K. Hayasaka,[26] H. Hayashii,[27] M. Hazumi,[10] D. Heffernan,[36] T. Higuchi,[10] L. Hinz,[22] H. Hoedlmoser,[9] T. Hokuue,[26] Y. Horii,[51] Y. Hoshi,[50] K. Hoshina,[55] S. Hou,[28] W.-S. Hou,[30] Y. B. Hsiung,[30] H. J. Hyun,[21] Y. Igarashi,[10] T. Iijima,[26] K. Ikado,[26] K. Inami,[26] A. Ishikawa,[42] H. Ishino,[53] R. Itoh,[10] M. Iwabuchi,[6] M. Iwasaki,[52] Y. Iwasaki,[10] C. Jacoby,[22] N. J. Joshi,[48] M. Kaga,[26] D. H. Kah,[21] H. Kaji,[26] S. Kajiwara,[36] H. Kakuno,[52] J. H. Kang,[58] P. Kapusta,[31] S. U. Kataoka,[27] N. Katayama,[10] H. Kawai,[2] T. Kawasaki,[33] A. Kibayashi,[10] H. Kichimi,[10] H. J. Kim,[21] H. O. Kim,[46] J. H. Kim,[46] S. K. Kim,[44] Y. J. Kim,[6] K. Kinoshita,[3] S. Korpar,[24,17] Y. Kozakai,[26] P. Križan,[23,17] P. Krokovny,[10] R. Kumar,[37] E. Kurihara,[2] A. Kusaka,[52] A. Kuzmin,[1] Y.-J. Kwon,[58] J. S. Lange,[5] G. Leder,[14] J. Lee,[44] J. S. Lee,[46] M. J. Lee,[44] S. E. Lee,[44] T. Lesiak,[31] J. Li,[9] A. Limosani,[25] S.-W. Lin,[30] Y. Liu,[6] D. Liventsev,[16] J. MacNaughton,[10] G. Majumder,[48] F. Mandl,[14] D. Marlow,[40] T. Matsumura,[26] A. Matyja,[31] S. McOnie,[47] T. Medvedeva,[16] Y. Mikami,[51] W. Mitaroff,[14] K. Miyabayashi,[27] H. Miyake,[36] H. Miyata,[33] Y. Miyazaki,[26] R. Mizuk,[16] G. R. Moloney,[25] T. Mori,[26] J. Mueller,[39] A. Murakami,[42] T. Nagamine,[51] Y. Nagasaka,[11] Y. Nakahama,[52] I. Nakamura,[10] E. Nakano,[35] M. Nakao,[10] H. Nakayama,[52] H. Nakazawa,[28] Z. Natkaniec,[31] K. Neichi,[50] S. Nishida,[10] K. Nishimura,[9] Y. Nishio,[26] I. Nishizawa,[54] O. Nitoh,[55] S. Noguchi,[27] T. Nozaki,[10] A. Ogawa,[41] S. Ogawa,[49] T. Ohshima,[26] S. Okuno,[18] S. L. Olsen,[9] S. Ono,[53] W. Ostrowicz,[31] H. Ozaki,[10] P. Pakhlov,[16] G. Pakhlova,[16] H. Palka,[31] C. W. Park,[46] H. Park,[21] K. S. Park,[46] N. Parslow,[47] L. S. Peak,[47] M. Pernicka,[14] R. Pestotnik,[17] M. Peters,[9] L. E. Piilonen,[57] A. Poluektov,[1] J. Rorie,[9] M. Rozanska,[31] H. Sahoo,[9] Y. Sakai,[10] H. Sakamoto,[20] H. Sakaue,[35] T. R. Sarangi,[6] N. Satoyama,[45] K. Sayeed,[3] T. Schietinger,[22] O. Schneider,[22] P. Schönmeier,[51] J. Schümann,[10] C. Schwanda,[14] A. J. Schwartz,[3] R. Seidl,[12,41] A. Sekiya,[27] K. Senyo,[26] M. E. Sevior,[25] L. Shang,[13] M. Shapkin,[15] C. P. Shen,[13] H. Shibuya,[49] S. Shinomiya,[36] J.-G. Shiu,[30] B. Shwartz,[1] J. B. Singh,[37] A. Sokolov,[15] E. Solovieva,[16] A. Somov,[3] S. Stanič,[34] M. Starič,[17] J. Stypula,[31] A. Sugiyama,[42] K. Sumisawa,[10] T. Sumiyoshi,[54] S. Suzuki,[42] S. Y. Suzuki,[10] O. Tajima,[10] F. Takasaki,[10] K. Tamai,[10] N. Tamura,[33] M. Tanaka,[10] N. Taniguchi,[20] G. N. Taylor,[25] Y. Teramoto,[35] I. Tikhomirov,[16] K. Trabelsi,[10] Y. F. Tse,[25] T. Tsuboyama,[10] K. Uchida,[9]

Y. Uchida,[6] S. Uehara,[10] K. Ueno,[30] T. Uglov,[16] Y. Unno,[8] S. Uno,[10] P. Urquijo,[25] Y. Ushiroda,[10] Y. Usov,[1] G. Varner,[9] K. E. Varvell,[47] K. Vervink,[22] S. Villa,[22] A. Vinokurova,[1] C. C. Wang,[30] C. H. Wang,[29] J. Wang,[38] M.-Z. Wang,[30] P. Wang,[13] X. L. Wang,[13] M. Watanabe,[33] Y. Watanabe,[18] R. Wedd,[25] J. Wicht,[22] L. Widhalm,[14] J. Wiechczynski,[31] E. Won,[19] B. D. Yabsley,[47] A. Yamaguchi,[51] H. Yamamoto,[51] M. Yamaoka,[26] Y. Yamashita,[32] M. Yamauchi,[10] C. Z. Yuan,[13] Y. Yusa,[57] C. C. Zhang,[13] L. M. Zhang,[43] Z. P. Zhang,[43] V. Zhilich,[1] V. Zhulanov,[1] A. Zupanc,[17] and N. Zwahlen[22]

(The Belle Collaboration)

[1]*Budker Institute of Nuclear Physics, Novosibirsk*
[2]*Chiba University, Chiba*
[3]*University of Cincinnati, Cincinnati, Ohio 45221*
[4]*Department of Physics, Fu Jen Catholic University, Taipei*
[5]*Justus-Liebig-Universität Gießen, Gießen*
[6]*The Graduate University for Advanced Studies, Hayama*
[7]*Gyeongsang National University, Chinju*
[8]*Hanyang University, Seoul*
[9]*University of Hawaii, Honolulu, Hawaii 96822*
[10]*High Energy Accelerator Research Organization (KEK), Tsukuba*
[11]*Hiroshima Institute of Technology, Hiroshima*
[12]*University of Illinois at Urbana-Champaign, Urbana, Illinois 61801*
[13]*Institute of High Energy Physics, Chinese Academy of Sciences, Beijing*
[14]*Institute of High Energy Physics, Vienna*
[15]*Institute of High Energy Physics, Protvino*
[16]*Institute for Theoretical and Experimental Physics, Moscow*
[17]*J. Stefan Institute, Ljubljana*
[18]*Kanagawa University, Yokohama*
[19]*Korea University, Seoul*
[20]*Kyoto University, Kyoto*
[21]*Kyungpook National University, Taegu*
[22]*Ecole Polytécnique Fédérale Lausanne, EPFL, Lausanne*
[23]*University of Ljubljana, Ljubljana*
[24]*University of Maribor, Maribor*
[25]*University of Melbourne, School of Physics, Victoria 3010*
[26]*Nagoya University, Nagoya*
[27]*Nara Women's University, Nara*
[28]*National Central University, Chung-li*
[29]*National United University, Miao Li*
[30]*Department of Physics, National Taiwan University, Taipei*
[31]*H. Niewodniczanski Institute of Nuclear Physics, Krakow*
[32]*Nippon Dental University, Niigata*
[33]*Niigata University, Niigata*
[34]*University of Nova Gorica, Nova Gorica*
[35]*Osaka City University, Osaka*
[36]*Osaka University, Osaka*
[37]*Panjab University, Chandigarh*

[38]Peking University, Beijing
[39]University of Pittsburgh, Pittsburgh, Pennsylvania 15260
[40]Princeton University, Princeton, New Jersey 08544
[41]RIKEN BNL Research Center, Upton, New York 11973
[42]Saga University, Saga
[43]University of Science and Technology of China, Hefei
[44]Seoul National University, Seoul
[45]Shinshu University, Nagano
[46]Sungkyunkwan University, Suwon
[47]University of Sydney, Sydney, New South Wales
[48]Tata Institute of Fundamental Research, Mumbai
[49]Toho University, Funabashi
[50]Tohoku Gakuin University, Tagajo
[51]Tohoku University, Sendai
[52]Department of Physics, University of Tokyo, Tokyo
[53]Tokyo Institute of Technology, Tokyo
[54]Tokyo Metropolitan University, Tokyo
[55]Tokyo University of Agriculture and Technology, Tokyo
[56]Toyama National College of Maritime Technology, Toyama
[57]Virginia Polytechnic Institute and State University, Blacksburg, Virginia 24061
[58]Yonsei University, Seoul

Abstract

We have measured branching fractions of hadronic τ decays involving an η meson using 485 fb^{-1} of data collected with the Belle detector at the KEKB asymmetric-energy e^+e^- collider. We obtain the following branching fractions: $\mathcal{B}(\tau^- \to K^-\eta\nu_\tau) = (1.62 \pm 0.05 \pm 0.09) \times 10^{-4}$, $\mathcal{B}(\tau^- \to K^-\pi^0\eta\nu_\tau) = (4.7 \pm 1.1 \pm 0.4) \times 10^{-5}$, $\mathcal{B}(\tau^- \to \pi^-\pi^0\eta\nu_\tau) = (1.39 \pm 0.03 \pm 0.07) \times 10^{-3}$, and $\mathcal{B}(\tau^- \to K^{*-}\eta\nu_\tau) = (1.13 \pm 0.19 \pm 0.07) \times 10^{-4}$ improving the accuracy compared to the best previous measurements by factors of six, eight, four and four, respectively.

PACS numbers:

INTRODUCTION

Hadronic decays of τ lepton provide a useful tool for studying QCD phenomena at low energy. Various decay modes including η meson(s) are interesting for testing the Wess-Zumino-Witten (WZW) anomaly [1, 2], chiral theory [3, 4], and relations to e^+e^- cross sections following from the conservation of the vector current (CVC) [5].

We measure the branching fractions of $\tau^- \to K^-\eta\nu_\tau$ (unless specified otherwise, charge conjugate decays are implied throughout the paper), $K^-\pi^0\eta\nu_\tau$, and $\pi^-\pi^0\eta\nu_\tau$ decays, and that of $\tau^- \to K^{*-}(892)\eta\nu_\tau$; the latter is evaluated from the corresponding $K^-\pi^0\eta\nu_\tau$ measurement. Studies of these modes have been reported by CLEO [6, 7, 8] and ALEPH [9], however, most of the results are based on rather low statistics, which do not allow one to discriminate between different theoretical predictions. We use a data sample with an integrated luminosity of 485 fb^{-1}, corresponding to production of 430 million τ-pairs collected with the Belle detector at the KEKB asymmetric-energy e^+e^- collider [10].

The Belle detector is a large-solid-angle magnetic spectrometer that consists of a silicon vertex detector (SVD), a 50-layer central drift chamber (CDC), an array of aerogel threshold Cherenkov counters (ACC), a barrel-like arrangement of time-of-flight scintillation counters (TOF), and an electromagnetic calorimeter comprised of CsI(Tl) crystals (ECL) located inside a superconducting solenoid coil that provides a 1.5 T magnetic field. An iron flux-return located outside the coil is instrumented to detect K_L^0 mesons and identify muons (KLM). The detector is described in detail elsewhere [11]. Two inner detector configurations were used. A 2.0 cm radius beampipe and a 3-layer silicon vertex detector were used for the first sample of 144 fb^{-1}, while a 1.5 cm radius beampipe, a 4-layer silicon detector and a small-cell inner drift chamber were used to record the remaining 341 fb^{-1}[12].

In this analysis, we use a data sample 100 times larger than any of the previous measurements. In addition, peaking backgrounds are estimated precisely to decrease systematic uncertainties.

A study of resonance formation in the hadronic final states is in progress and will be reported later.

EVENT SELECTION

Candidate $e^+e^- \to \tau^+\tau^-$ events are selected with the following common properties:

$$e^+e^- \to \tau^+_{\rm tag}\tau^-_{\rm sig}$$
$$\tau^-_{\rm sig} \to X\eta\nu_\tau \quad \text{and} \quad \tau^+_{\rm tag} \to (e/\mu)^+\nu_l\bar{\nu_\tau},$$

where X denotes K^-, $K^-\pi^0$, or $\pi^-\pi^0$. Candidate η mesons are reconstructed through two decay modes: $\gamma\gamma$ with a branching fraction of $39.39 \pm 0.24\%$ or $\pi^+\pi^-\pi^0$ with a branching fraction of $22.68 \pm 0.35\%$ with $\pi^0 \to \gamma\gamma$. In order to remove $q\overline{q}$ contamination, the tag-side τ is required to decay leptonically i.e. $\tau^- \to \ell^-\nu_\tau\bar{\nu}_l$ ($\ell = e/\mu$) (with a branching fraction of $35.20 \pm 0.07\%$). All branching fractions are taken from Ref. [13].

$\underline{\tau^- \to K^-\eta\nu_\tau \text{ selection}}$

A candidate event is required to contain either two charged tracks with zero net charge and at least two γ's in the $\eta \to \gamma\gamma$ case, or four charged tracks with zero net charge and at least two γ's in the $\eta \to \pi^+\pi^-\pi^0$ ($\pi^0 \to \gamma\gamma$) case. A charged track should have transverse

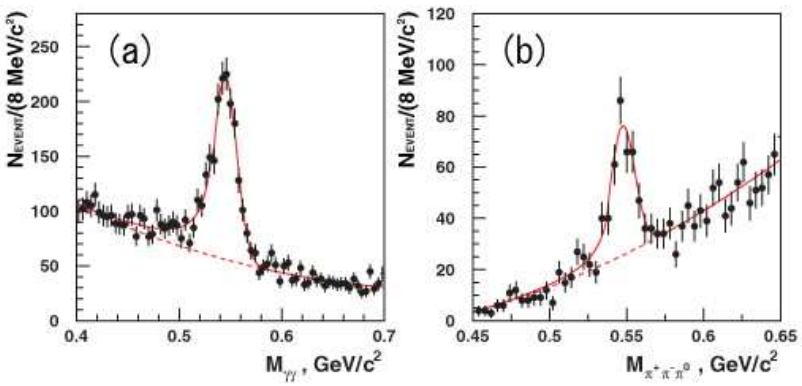

FIG. 1: $M_{\gamma\gamma}$ distributions for $K^-\eta\nu_\tau$ selection in (a) $\eta \to \gamma\gamma$ and (b) $\eta \to \pi^-\pi^+\pi^0$ decays. Data are fit with a Crystal Ball function plus a second-order polynomial for the background (BG). The best fit result is indicated by the solid curve with the BG shown by the dashed curve.

momentum, $p_t > 0.1$ GeV/c, and $-0.866 < \cos\theta < 0.956$ (θ is the polar angle within the detector aperture) where p_t and θ are measured relative to the direction opposite to that of the incident e^+ beam in the laboratory frame, and the γ should have energy $E_\gamma > 0.05$ GeV within the same polar angle fiducial region as above.

To select a sample of τ-pairs, the thrust vector and total energy in the center-of-mass system are required to satisfy $|V_{\rm thrust}| > 0.8$ and $3.0 < E^{\rm CM}_{\rm total} < 10.0$ GeV, respectively. Each event is then subdivided perpendicularly to the thrust axis into two hemispheres, the signal and the tag. To reduce $q\overline{q}$ contamination the effective mass of the particles on the tag side should satisfy the requirements, $M_{\rm tag} < m_\tau$ (1.78 GeV/c^2), while on the signal side the mass, $M_{\rm sig}$, should satisfy 0.70 GeV/c^2 $< M_{\rm sig} < m_\tau$.

To reconstruct an η from 2γ's, two γ's with $E_\gamma > 0.2$ GeV are required in the barrel region ($-0.624 < \cos\theta < 0.833$) with at most one γ with $0.05 < E_\gamma < 0.2$ GeV in the endcap region to allow for initial state radiation. In order to reduce incorrect combinations with a γ from a π^0 decay (denoted hereafter as γ_{π^0}), the η-candidate γ (γ_η) should not form a π^0 mass with any other γ (π^0 veto selection). In this analysis the π^0 mass window is defined as 0.105 GeV/c^2 $< M_{\gamma\gamma} < 0.165$ GeV/c^2 (a $\pm 3\sigma$ range in the detector resolution). Particle identification (PID) uses a likelihood ratio, $\mathcal{P}_x$, for a charged particle of species x ($x = \mu,\ e,\ K,$ or π). $\mathcal{P}_x$ is defined as $\mathcal{P}_x = L_x/\Sigma_y L_y$ (the sum runs over the relevant particle species), where L_x is a likelihood based on the energy deposit and shower shape in the ECL, the momentum and dE/dX measured by the CDC, the particle range in the KLM, the light yield in the ACC, and particle's time-of-flight from the TOF counter [14]. For the track on the tag side, $\mathcal{P}_e > 0.8$ for an e candidate and $\mathcal{P}_\mu > 0.8$ for a μ candidate with $p > 0.7$ GeV/c. On the other hand, a kaon is identified as a track satisfying not only $\mathcal{P}_K > 0.9$, but also $\mathcal{P}_e < 0.2$ in order to suppress two-photon events, with $p > 0.3$ GeV/c.

We also include correlations between tracks and γ's. The polar angle of the missing momentum that must be attributed to neutrinos, should satisfy $-0.866 < \cos\theta(P_{\rm miss}) < 0.956$. The opening angle between the K^- and η satisfies the requirement, $\cos\theta(P^{\rm CM}_K; P^{\rm CM}_\eta) > 0.8$. The opening angle and energy of two γ_η's should satisfy the following condition: $0.5 < \cos\theta(P^{\rm CM}_{\gamma 1}; P^{\rm CM}_{\gamma 2}) < 0.96$ and $(E^{\rm CM}_{\gamma 1} - E^{\rm CM}_{\gamma 2})/(E^{\rm CM}_{\gamma 1} + E^{\rm CM}_{\gamma 2}) < 0.8$, respectively.

The $\gamma\gamma$ mass distribution obtained after these requirements is shown in Fig. 1 (a).

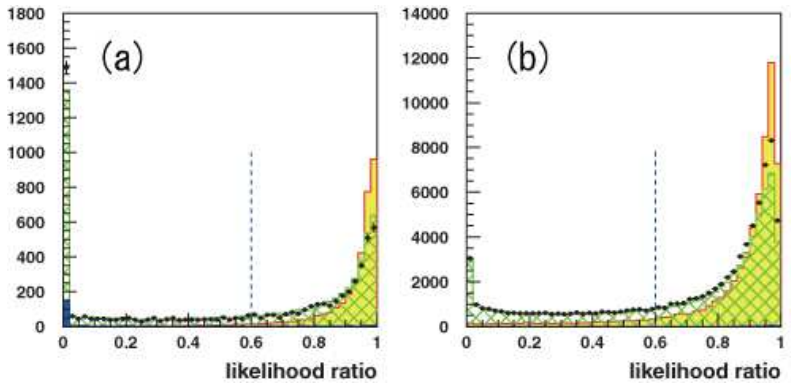

FIG. 2: Distribution of likelihood ratios for (a) $K^-\pi^0\eta\nu_\tau$ and (b) $\pi^-\pi^0\eta\nu_\tau$ candidates. The points with error bars are the data. The yellow, green hatched, and blue histograms indicate the signal, $\tau\tau$ background, and $q\overline{q}$ background MC distributions, respectively. The MC histograms are normalized to the integrated luminosity of the data. For demonstration purposes, the branching fractions of signal MC decays are set to 10^{-3} and 10^{-2} for (a) and (b), respectively. The dashed vertical line show the likelihood ratio requirement.

In the case of $\eta \to \pi^+\pi^-\pi^0$ reconstruction, candidate events should have two additional charged tracks compared to the $\eta \to \gamma\gamma$ sample, but two of the γ's have to form a π^0 instead of an η. While this mode provides one more constraint compared to those in the previous case improving the background rejection, the higher multiplicity reduces the detection efficiency.

The selection criteria different from those in the previous case are indicated below. π^+ and π^- candidates are required to have $0.3\ \mathrm{GeV}/c < p < 2.0\ \mathrm{GeV}/c$ and to be inconsistent with the e hypothesis ($\mathcal{P}_e < 0.2$) to reject the two-photon background. The photons used to form π^0-candidates are required to have $E_\gamma > 0.1$ GeV. In order to remove the contributions from higher mass states such as decays of an ω meson, the condition $M_{\pi^+\pi^-\pi^0} < 0.7\ \mathrm{GeV}/c^2$ is imposed. The condition on the polar angle of the missing momentum is the same as in the previous case while the π^0 momentum should be $P^{\mathrm{CM}}_{\pi^0} > 0.5\ \mathrm{GeV}/c$.

The resulting $\pi^+\pi^-\pi^0$ mass distribution is shown in Fig.1 (b).

Selection of $\tau^- \to K^-\pi^0\eta\nu_\tau$ and $\pi^-\pi^0\eta\nu_\tau$

For these τ decay modes, we use only $\eta \to \gamma\gamma$ to reconstruct the η, because of the small detection efficiency for $\eta \to \pi^+\pi^-\pi^0$. Correspondingly, a candidate event should contain two charged tracks and at least four γ's.

The selection criteria different from those for $K^-\eta\nu_\tau$ are listed below. The total momentum on the signal side is required to satisfy $\sum P^{\mathrm{CM}}_{\mathrm{sig}} > 2.5\ \mathrm{GeV}/c$; two additional γ's are required to lie in the barrel region on the signal side that form the π^0 mass; a condition on cosine of the opening angle between the missing momentum and the direction of the thrust axis pointing to the signal side is imposed: $\cos\theta(P^{\mathrm{CM}}_{\mathrm{miss}}; P^{\mathrm{CM}}_{\mathrm{thrust}}) < -0.6$. For the $\pi^-\pi^0\eta\nu_\tau$ mode, π^- candidates should have $\mathcal{P}_K < 0.2$ and $\mathcal{P}_e < 0.2$.

To further suppress backgrounds, we apply a likelihood selection using seven variables, such as $|V_{\mathrm{thrust}}|$, P^{CM}_η, M^2_{miss} (missing mass squared), $P^{\mathrm{CM}}_{\pi^0}$, $E^{\mathrm{CM}}_{\gamma_\eta}$, $\sum P^{\mathrm{CM}}_{\mathrm{sig}}$, and $\cos\theta(P^{\mathrm{CM}}_{K/\pi}; P^{\mathrm{CM}}_\eta)$. The $\tau\tau$ background MC is used for the background likelihood while the distributions from $K^-\pi^0\eta\nu$ and $\pi^-\pi^0\eta\nu$ MC are used for the signal likelihood in each case.

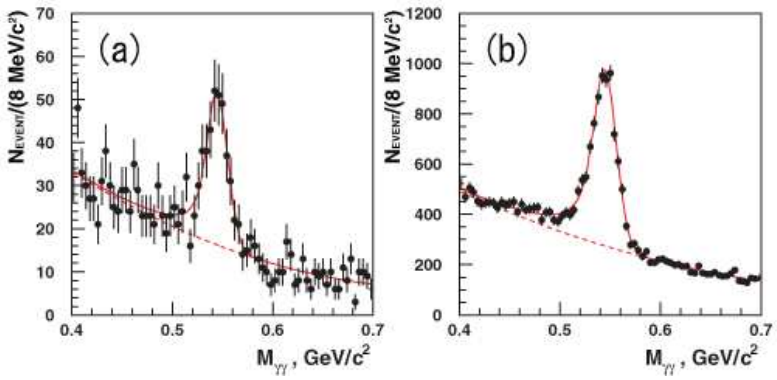

FIG. 3: $M_{\gamma\gamma}$ distributions for (a) $K^-\pi^0\eta\nu_\tau$ and (b) $\pi^-\pi^0\eta\nu_\tau$ candidates. Data are fit with a Crystal Ball function plus a second-order polynomial for the background (BG). The result of the best fit is indicated by the solid curve with the BG shown by the dashed curve.

The resulting likelihood ratios defined for $K^-\pi^0\eta\nu_\tau$ and $\pi^-\pi^0\eta\nu_\tau$ are shown in Figs.2 (a) and (b), respectively. About half of the background is removed while 93% and 90% of the signal is retained for each of the respective modes.

The obtained $M_{\gamma\gamma}$ distributions are shown in Figs. 3 (a) and (b) for the $K^-\pi^0\eta\nu_\tau$ and $\pi^-\pi^0\eta\nu_\tau$ modes, respectively.

BRANCHING FRACTIONS FOR $K^-\eta\nu_\tau$, $K^-\pi^0\eta\nu_\tau$ AND $\pi^-\pi^0\eta\nu_\tau$ DECAYS

To determine the signal yields we determine the number of η's and then subtract cross-feeds. In order to extract the number of η's from the resulting $M_{\gamma\gamma}$ distributions, Figs. 1 and 3, we use the Crystal Ball function [15] to represent the η signal and a second-order polynomial for the background distribution. The result of the fits is indicated by the solid curve in the corresponding figures. The best fits give an η mass, m_η, of 0.545 ± 0.001 GeV/c^2, in good agreement with the PDG value of 0.54751 ± 0.00018 GeV/c^2, and a resolution $\sigma_{m_\eta} = 0.012 \pm 0.002$ GeV/c^2 for the three different decay modes in the $\eta \to \gamma\gamma$ case and $m_\eta = 0.5474 \pm 0.0007$ GeV/c^2 with $\sigma_{m_\eta} = 0.0075 \pm 0.0004$ GeV/c^2 for the $K^-\eta\nu_\tau$ mode in the $\eta \to \pi^+\pi^-\pi^0$ case.

The η yields obtained from the fits are $N_{K^-\eta\nu_\tau} = 1387 \pm 43$, $N_{K^-\pi^0\eta\nu_\tau} = 270 \pm 33$, and $N_{\pi^-\pi^0\eta\nu_\tau} = 5959 \pm 105$ events for the $K^-\eta\nu_\tau$, $K^-\pi^0\eta\nu_\tau$, and $\pi^-\pi^0\eta\nu_\tau$ modes, respectively, in the $\eta \to \gamma\gamma$ case. The yield for the $\eta \to \pi^+\pi^-\pi^0$ case is $N_{K^-\eta\nu_\tau;\eta\to3\pi} = 241 \pm 21$ events. The η signal region is defined as 0.48 GeV/c^2 $< M_{\gamma\gamma} <$ 0.58 GeV/c^2 in the $\eta \to \gamma\gamma$ case while it is 0.52 GeV/c^2 $< M_{\pi^+\pi^-\pi^0} <$ 0.58 GeV/c^2 in the $\eta \to \pi^+\pi^-\pi^0$ case. The detection efficiencies are estimated with MC simulation in the same manner as the detection of η yields. The corresponding efficiencies are $\varepsilon = 0.94$ %, 0.35 %, 0.47 %, and 0.16 %, respectively, and include the intermediate branching fractions such as $\mathcal{B}(\eta \to \gamma\gamma)$, $\mathcal{B}(\eta \to \pi^+\pi^-\pi^0)$, and $\mathcal{B}(\tau^- \to l^-\nu_\tau\bar{\nu}_l)$.

These event yields include backgrounds classified into three categories. One is due to cross-feed effects between the three signal modes, which is taken into account by solving the following system of equations:

$$N_{K^-\eta\nu_\tau} = 2N_{\tau\tau}(\mathcal{B}(K^-\eta\nu_\tau)\cdot\epsilon_1^1 + \mathcal{B}(K^-\pi^0\eta\nu_\tau)\cdot\epsilon_2^1 + \mathcal{B}(\pi^-\pi^0\eta\nu_\tau)\cdot\epsilon_3^1), \quad (1)$$

TABLE I: Raw η yields for the four selected τ decay modes. N_η is the total number of η events detected, which include cross-feed from two other modes. The contributions of $q\overline{q}$ and 'other', mostly $\pi^-\pi^0\pi^0\eta\nu_\tau$ and $\pi^-\pi^+\pi^-\eta\nu_\tau$, are also included.

Mode	N_η	$K\eta\nu_\tau$	$K\pi^0\eta\nu_\tau$	$\pi\pi^0\eta\nu_\tau$	Other	$q\bar{q}$
$K^-\eta\nu_\tau$ $(\eta\to\gamma\gamma)$	1387 ± 43	$-$	15.1 ± 3.8	18.0 ± 1.0	1.1 ± 0.2	30.6 ± 15.6
$K^-\pi^0\eta\nu_\tau$	270 ± 33	16.0 ± 0.9	$-$	85.3 ± 4.6	1.2 ± 0.4	27.0 ± 8.5
$\pi^-\pi^0\eta\nu_\tau$	5959 ± 105	2.4 ± 0.1	9.4 ± 2.4	$-$	71.6 ± 20	212 ± 29
$K^-\eta\nu_\tau$ $(\eta\to\pi^+\pi^-\pi^0)$	241 ± 21	$-$	3.3 ± 0.8	5.8 ± 1.3	<1.18	9.1 ± 2.2

$$N_{K^-\pi^0\eta\nu_\tau} = 2N_{\tau\tau}(\mathcal{B}(K^-\eta\nu_\tau)\cdot\epsilon_1^2 + \mathcal{B}(K^-\pi^0\eta\nu_\tau)\cdot\epsilon_2^2 + \mathcal{B}(\pi^-\pi^0\eta\nu_\tau)\cdot\epsilon_3^2), \quad (2)$$

$$N_{\pi^-\pi^0\eta\nu_\tau} = 2N_{\tau\tau}(\mathcal{B}(K^-\eta\nu_\tau)\cdot\epsilon_1^3 + \mathcal{B}(K^-\pi^0\eta\nu_\tau)\cdot\epsilon_2^3 + \mathcal{B}(\pi^-\pi^0\eta\nu_\tau)\cdot\epsilon_3^3), \quad (3)$$

where $\mathcal{B}(K^-\eta\nu_\tau)$, $\mathcal{B}(K^-\pi^0\eta\nu_\tau)$, and $\mathcal{B}(\pi^-\pi^0\eta\nu_\tau)$ are the branching fractions of the respective modes and $N_{\tau\tau}$ is the total number of τ pairs produced. Here ε_j^i is the detection efficiency in each case and j (i) indicates the decay sample (selection criteria).

The second type of background is from decay modes of the τ-lepton itself, such as $\pi^-\pi^0\pi^0\eta\nu_\tau$ and $\pi^-\pi^+\pi^-\eta\nu_\tau$. These backgrounds are estimated by using a $\tau\tau$ MC simulation with branching fractions taken from [16]. The estimated background is included in the 'other' category in Table I. The contribution of this type of background is negligible for the $K^-\eta\nu_\tau$ and $K^-\pi^0\eta\nu_\tau$ modes, and is smaller than the statistical uncertainty in the η yield obtained above for the $\pi^-\pi^0\eta\nu_\tau$ mode. The contamination from $\pi^-\eta\nu_\tau$ decay should also be considered. This decay is strongly suppressed since it violates G-parity and proceeds via a second-class current. Its branching fraction is predicted to be 10^{-5}. Therefore, its contribution to each mode is negligible.

The last background category is $e^+e^-\to q\bar{q}$, which is estimated from MC simulation. The MC was tuned beforehand and validated with a $q\bar{q}$ enriched sample, which was produced with some variations of the event selection criteria. The $M_{\rm sig}$ cut is removed and the condition $M_{\rm tag} > m_\tau$ is implemented on the tag side. In addition, the PID requirement for the charged track on the tag side was reversed (i.e. $\mathcal{P}_e < 0.8$ and $\mathcal{P}_\mu < 0.8$). The η yield of MC was then tuned to be consistent with that of data. The $q\bar{q}$ contributions are 2-4 % of the η yields for the $K^-\eta\nu_\tau$ and $\pi^-\pi^0\eta\nu_\tau$ modes and 10% for the $K^-\pi^0\eta\nu_\tau$. They also are summarized in Table I.

After subtracting the 'other' and $q\overline{q}$ contributions from the individual η yields, we solve the system of equations to obtain the branching fractions for three decay modes. They are $(1.62\pm0.05)\times10^{-4}$, $(4.7\pm1.1)\times10^{-5}$, and $(1.39\pm0.03)\times10^{-3}$ for $K^-\eta\nu_\tau$, $K^-\pi^0\eta\nu_\tau$, and $\pi^-\pi^0\eta\nu_\tau$, respectively. The cross-feed yields obtained are also listed in Table I. The number of cross-feed events for $K^-\eta\nu_\tau$ in the $\eta\to\pi^+\pi^-\pi^0$ case is evaluated using the above branching fractions, obtained in the $\eta\to\gamma\gamma$ case. The branching fraction for $K^-\eta\nu_\tau$ in this case is $(1.65\pm0.16)\times10^{-4}$.

The systematic uncertainties are estimated as follows: the estimation of peaking backgrounds provides sizable uncertainties only in case of the $\pi^-\pi^0\eta\nu_\tau$ (3.3 %) and $q\overline{q}$ (6.0 %) contributions to the $K^-\pi^0\eta\nu_\tau$ mode. As for the $q\bar{q}$ estimation, due to the finite statistics of $q\bar{q}$ enriched sample, the uncertainties of 26 %, 19 %, and 9.6 % for $K^-\eta\nu_\tau$, $K^-\pi^0\eta\nu_\tau$, and

TABLE II: Summary of systematic uncertainties in each mode (%)

Mode	$K^-\eta\nu_\tau$	$K^-\pi^0\eta\nu_\tau$	$\pi^-\pi^0\eta\nu_\tau$	$K^-\eta\nu_\tau$	$K^{*-}\eta\nu_\tau$
η detection	$\eta\to\gamma\gamma$	$\eta\to\gamma\gamma$	$\eta\to\gamma\gamma$	$\eta\to\pi^+\pi^-\pi^0$	$\eta\to\gamma\gamma$
Estimation of $K^-\eta\nu_\tau$	–	0.6	1.8×10^{-3}	–	–
Estimation of $K^-\pi^0\eta\nu_\tau$	0.3	–	4.2×10^{-2}	0.4	–
Estimation of $\pi^-\pi^0\eta\nu_\tau$	7.5×10^{-2}	3.3	–	0.1	–
Estimation of $\pi^-\pi^0\pi^0\eta\nu_\tau$	–	–	0.4	–	–
Estimation of $q\bar{q}$	1.5	6.0	0.5	1.5	2.4
Particle ID (K/π)	3.3	2.2	1.0	2.8	2.2
Particle ID (Lepton)	2.3	2.8	2.6	2.6	2.6
Track finding	1.3	1.3	1.3	3.3	1.3
Luminosity measurement	1.6	1.6	1.6	1.6	1.6
π^0 detection	–	2.0	2.0	2.0	2.0
π^0 veto	2.8	2.8	2.8	–	2.8
Signal MC	0.5	1.7	0.7	1.3	1.7
$\mathcal{B}(\eta\to\pi^+\pi^-\pi^0)$	–	–	–	1.6	–
Total	5.6	8.9	5.0	6.3	6.0

$\pi^-\pi^0\eta\nu_\tau$ decays arise from tuning, respectively. The errors in the $q\bar{q}$ background estimations in Table I come from this uncertainty and the statistical uncertainty in the $q\bar{q}$ MC, and are treated as systematic uncertainties. The uncertainties in the peaking backgrounds in all other cases are rather small. Uncertainties in the PID efficiency and fake rate are evaluated to be 2-3 % for kaon ID, 1 % for π ID and around 2.5 % for the lepton ID; these values are obtained by averaging the estimated uncertainties depending on momentum and polar angle of each charged track. For the π^0 veto selection, the efficiency was compared between data and MC with a sample in which the PID of the charged track on the tag side was reversed from the usual $\pi^-\pi^0\eta\nu_\tau$ selection. The efficiencies were consistent. Therefore, 2.8 % of the statistical uncertainty from this comparison was counted as systematic uncertainty. Other systematic uncertainties are summarized in Table II. The total systematic uncertainties are 5.6 %, 8.9 %, 5.0 %, and 6.3 % for the $K^-\eta\nu_\tau$ ($\eta\to\gamma\gamma$), $K^-\pi^0\eta\nu_\tau$, $\pi^-\pi^0\eta\nu_\tau$, and $K^-\eta\nu_\tau$ ($\eta\to\pi^+\pi^-\pi^0$) modes, respectively.

Taking the systematic uncertainties into account we obtain the following branching fractions:

$$\begin{aligned}
\mathcal{B}(\tau^-\to K^-\eta\nu_\tau) &= (1.62\pm0.05\pm0.09)\times10^{-4} \qquad \text{for } \eta\to\gamma\gamma,\\
&= (1.65\pm0.16\pm0.10)\times10^{-4} \qquad \text{for } \eta\to\pi^+\pi^-\pi^0,\\
\mathcal{B}(\tau^-\to K^-\pi^0\eta\nu_\tau) &= (4.7\ \pm1.1\pm0.4)\times10^{-5},\\
\mathcal{B}(\tau^-\to \pi^-\pi^0\eta\nu_\tau) &= (1.39\pm0.03\pm0.07)\times10^{-3}.
\end{aligned}$$

By combining two measurements for $\tau^-\to K^-\eta\nu_\tau$ decay, we obtain:

$$\mathcal{B}(\tau^-\to K^-\eta\nu_\tau) = (1.62\pm0.05\pm0.09)\times10^{-4}.$$

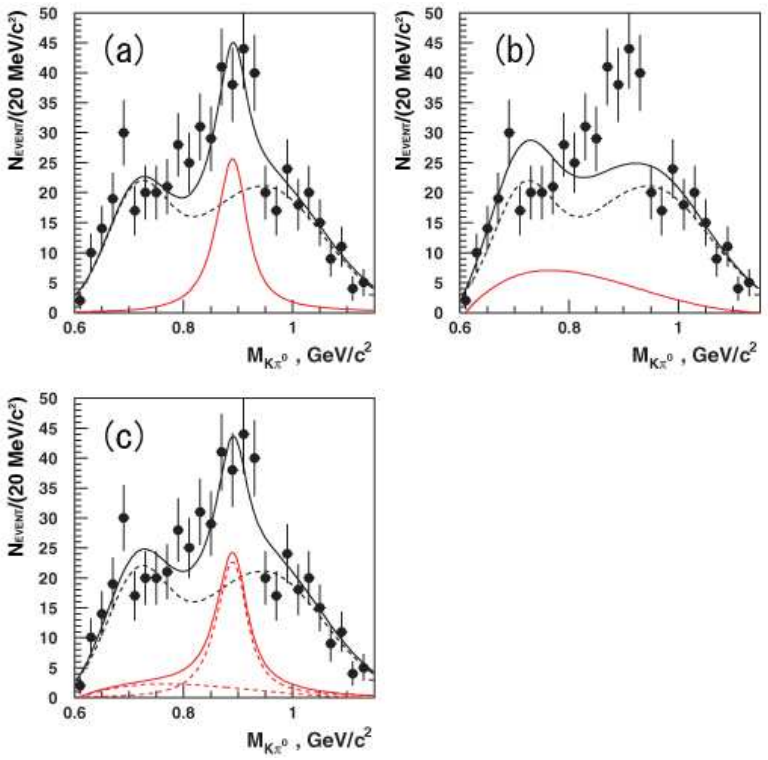

FIG. 4: The $K^-\pi^0$ invariant mass distribution for the $K^-\pi^0\eta\nu_\tau$ events. Data are fitted with a Breit-Wigner (BW) function in (a), and the best fit is indicated by the solid curve while the continuum component evaluated from sideband regions is shown by the dashed curve. The fit gives $N_{K^{*-}\eta\nu_\tau} = 119 \pm 19$ events with $\chi^2/(\text{d.o.f.} = 27) = 1.15$ (the probability to obtain this result is 0.265). (b) and (c) show the results of similar fit with a phase space distribution only and a BW plus a phase space distribution. In these cases the results are $N_{K^{*-}\eta\nu_\tau} = 102 \pm 21$ events with $\chi^2/(\text{d.o.f.} = 27) = 2.09$ (the probability is 0.0008) for the phase-space distribution, or $N_{K^{*-}\eta\nu_\tau} = 105 \pm 20$ and $N_{K^-\pi^0\eta\nu_\tau} = 33 \pm 30$ events with $\chi^2/(\text{d.o.f.} = 26) = 1.13$ (the probability is 0.294).

BRANCHING FRACTION FOR $K^{*-}(892)\eta\nu_\tau$

From the $K^-\pi^0\eta\nu_\tau$ samples within the η mass region, $0.50\ \text{GeV}/c^2 < M_{\gamma\gamma} < 0.58\ \text{GeV}/c^2$, we extract a branching fraction for $\tau^- \to K^{*-}(892)\eta\nu_\tau$ decay through the $K^{*-}(892) \to K^-\pi^0$ mode ($\mathcal{B}(K^{*-}(892) \to K^-\pi^0) = 1/3$).

The distribution of $K^-\pi^0$ invariant mass, $M_{K^-\pi^0}$, for the selected samples is shown in Fig. 4. The $\tau^- \to \pi^-\pi^0\eta\nu_\tau$ background, which cannot be neglected as shown in Table I, is estimated by using MC simulation with the branching fraction measured in this paper. The other backgrounds are estimated from two sidebands of the $M_{\gamma\gamma}$ distribution: $0.43\ \text{GeV}/c^2 < M_{\gamma\gamma} < 0.48\ \text{GeV}/c^2$ and $0.60\ \text{GeV}/c^2 < M_{\gamma\gamma} < 0.65\ \text{GeV}/c^2$. The background distribution is indicated by the dashed curve. The peculiar shape of the expected background is due to two components contributing to it: that of $\pi^-\pi^0\eta\nu_\tau$ at high mass and the one from all other τ decays at low mass. A clear excess above the background is seen around 0.9 GeV/c^2, suggesting $K^{*-}(892)$ resonance formation. Three types of signal

TABLE III: Comparison of our measurement with previous results

Mode	$\mathcal{B}$ in this analysis	Previous $\mathcal{B}$	Reference
$\tau^- \to K^-\eta\nu_\tau$	$(1.62 \pm 0.05 \pm 0.09) \times 10^{-4}$	$(2.6 \pm 0.5 \pm 0.5) \times 10^{-4}$	CLEO [7]
		$(2.9 \pm 1.3 \pm 0.7) \times 10^{-4}$	ALEPH [9]
$\tau^- \to K^-\pi^0\eta\nu_\tau$	$(4.7 \pm 1.1 \pm 0.4) \times 10^{-5}$	$(17.7 \pm 5.6 \pm 7.1) \times 10^{-5}$	CLEO [8]
$\tau^- \to \pi^-\pi^0\eta\nu_\tau$	$(1.39 \pm 0.03 \pm 0.07) \times 10^{-3}$	$(1.7 \pm 0.2 \pm 0.2) \times 10^{-3}$	CLEO [6]
		$(1.8 \pm 0.4 \pm 0.2) \times 10^{-3}$	ALEPH [9]
$\tau^- \to K^{*-}\eta\nu_\tau$	$(1.13 \pm 0.19 \pm 0.07) \times 10^{-4}$	$(2.90 \pm 0.80 \pm 0.42) \times 10^{-4}$	CLEO [8]

functions have been tested. A Breit-Wigner (BW) function whose mass and width are set to those of the $K^{*-}(892)$ is fitted to data in Fig. 4 (a). A fit with the hypothesis that the excess signal events are due to a non-resonant, but $V-A$ pure phase space process is shown in Fig. 4 (b). Figure 4 (c) shows the result of a fit with a BW plus a phase space function as a signal. In each case, the signal function is smeared to take into account the detector resolution. The BW function describes the data well in Fig. 4 (a) and the resulting number of $K^{*-}(892)$ events is $N_{K^{*-}\eta\nu_\tau} = 119 \pm 19$. In contrast, the fit shown in Fig. 4 (b) is in complete disagreement with the data. Although inclusion of a small phase space component in addition to the dominant K^{*-} resonance component also represents data well as shown in Fig. 4 (c), the resulting magnitude of the phase space component is consistent with zero within errors. Therefore, we conclude that all excess events are produced via the $K^{*-}(892)$ resonance.

The detection efficiency is evaluated by MC simulation to be $\varepsilon = 0.12\%$, including the branching fractions of $\mathcal{B}(K^{*-}(892) \to K^-\pi^0)$, $\mathcal{B}(\eta \to \gamma\gamma)$, and $\mathcal{B}(\tau \to \ell\nu_\tau\overline{\nu})$.

Since the requirement of $K^{*-}(892)$ formation in this case is a rather strong constraint, no significant peaking background contribution from other τ decays is found. Therefore, the systematic uncertainty in the $K^{*-}(892)\eta\nu_\tau$ mode is small as compared with the $K^-\pi^0\eta\nu_\tau$ analysis. Other sources of systematic uncertainties are the same as those of $K^-\pi^0\eta\nu_\tau$, except for the background contamination; a total systematic uncertainty of 6.0 % is obtained with details summarized in Table II. Finally, we obtain the following branching fraction:

$$\mathcal{B}(\tau^- \to K^{*-}\eta\nu_\tau) = (1.13 \pm 0.19 \pm 0.07) \times 10^{-4}. \quad (4)$$

RESULTS AND DISCUSSION

We have obtained branching fractions for four different decay modes based on a high-statistics data sample of 430 million τ-pairs collected with the Belle detector:

$$\begin{aligned}
\mathcal{B}(\tau^- \to K^-\eta\nu_\tau) &= (1.62 \pm 0.05 \pm 0.09) \times 10^{-4}, \\
\mathcal{B}(\tau^- \to K^-\pi^0\eta\nu_\tau) &= (4.7 \pm 1.1 \pm 0.4) \times 10^{-5}, \\
\mathcal{B}(\tau^- \to \pi^-\pi^0\eta\nu_\tau) &= (1.39 \pm 0.03 \pm 0.07) \times 10^{-3}, \\
\mathcal{B}(\tau^- \to K^{*-}\eta\nu_\tau) &= (1.13 \pm 0.19 \pm 0.07) \times 10^{-4},
\end{aligned}$$

where the first error is statistical and the second is systematic.

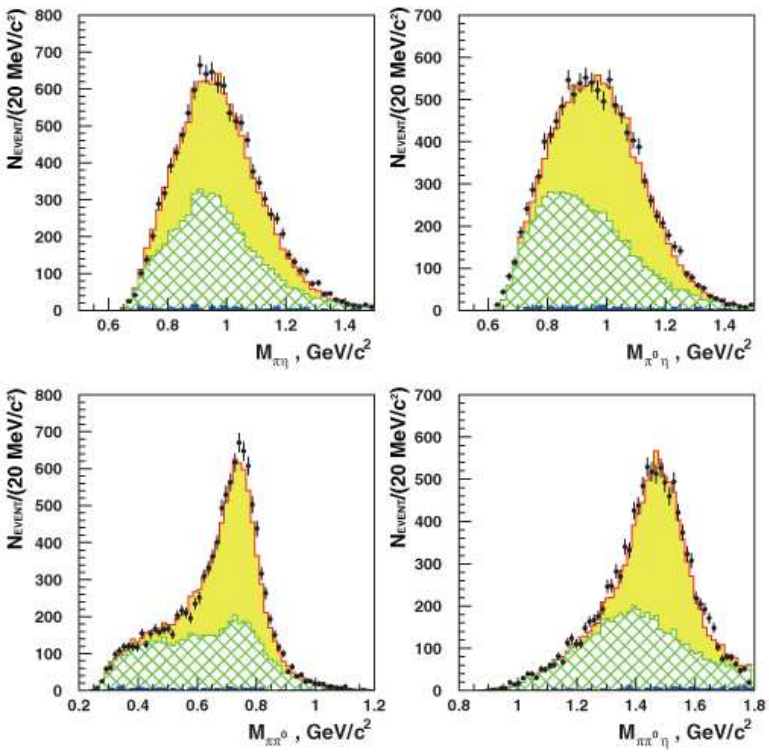

FIG. 5: The invariant mass distributions of various combinations of final state particles for $\tau^- \to \pi^-\pi^0\eta\nu_\tau$ decay. The points with error bars are the data. The yellow, green hatched, and blue histograms indicate the signal, $\tau\tau$ background, and $q\overline{q}$ background MC distributions, respectively. The dominant backgrounds come from $\tau\tau$ events. The $q\overline{q}$ background is strongly suppressed and negligible in our sample.

Compared to previous experiments, we have improved not only the statistical uncertainties, but also evaluated reliably the background contamination. In Table III our results are compared to those previously obtained by the CLEO [6, 7, 8] and ALEPH [9] collaborations. Our measurement improves the uncertainties in the branching fractions by a factor of six ($K^-\eta\nu_\tau$), eight ($K^-\pi^0\eta\nu_\tau$), four ($\pi^-\pi^0\eta\nu_\tau$), and four ($K^{*-}\eta\nu_\tau$) compared to the most precise determinations from CLEO. In addition, the high statistics of our experiment allows much more reliable estimation of various backgrounds including the peaking one. The relatively poor statistics of previous measurements imposed some limitations on BG estimations [17]. It is also noteworthy that in all cases the central value of our measurement is lower than that of the other measurements. This may be due to the underestimation of backgrounds in the previous experiments. The improved accuracy in the branching fractions of the decay modes reported here is important for future searches for the second-class current $\tau^- \to \pi^-\eta\nu_\tau$ decay.

Our branching fraction for $\tau^- \to \pi^-\pi^0\eta\nu_\tau$ decay is consistent with the prediction based on CVC and experimentally measured $e^+e^- \to \pi^+\pi^-\eta$ cross sections [5]. In addition, the Monte Carlo code TAUOLA reproduces the observed hadronic mass distributions rather well as shown in Fig. 5 while more tuning is needed for τ's decay modes involving kaon(s). The values of the branching fractions obtained for $\tau^- \to K^-\eta\nu_\tau$ and $\tau^- \to K^-\pi^0\eta\nu_\tau$ decays

differ slightly from the predictions by Li [4].

Further studies of final state dynamics and resonance formation in the $\tau^- \to K^-\pi^0\eta\nu_\tau$ and $\pi^-\pi^0\eta\nu_\tau$ decays, which may be important for understanding the WZW anomaly are in progress.

---

[1] J. Wess and B. Zumino, Phys. Lett. B **37** (1971) 95.
[2] E. Witten, Nucl. Phys. B **223** (1983) 422.
[3] A. Pich, Phys. Lett. B **196** (1987) 561.
[4] B. A. Li, Phys. Rev. D **55** (1997) 1436.
[5] S. Eidelman and V. Ivanchenko, Phys. Lett. B **257** (1991) 437.
[6] CLEO Collaboration, M. Artuso et al., Phys. Rev. Lett. **69** (1992) 3278.
[7] CLEO Collaboration, J. Bartelt et al., Phys. Rev. Lett. **76** (1996) 4119.
[8] CLEO Collaboration, M. Bishai et al., Phys. Rev. Lett. **82** (1999) 281.
[9] ALEPH Collaboration, D. Buskulic et al., Z. Phys. C **74** (1997) 263.
[10] S. Kurokawa and E. Kikutani, Nucl. Instr. and. Meth. A **499** (2003) 1, and other papers included in this volume.
[11] Belle Collaboration, A. Abashian et al., Nucl. Instr. and Meth. A **479** (2002) 117.
[12] Z. Natkaniec *et al.* (Belle SVD2 Group), Nucl. Instr. and Meth. A **560** (2006) 1.
[13] W.-M. Yao et al., J. Phys. G **33** (2006) 1, and 2007 partial update for edition 2008.
[14] K. Hanagaki et al., Nucl. Instr. and Meth. A **485** (2002) 490;
A. Abashian et al., Nucl. Instr. and Meth. A **491** (2002) 69;
E. Nakano et al., Nucl. Instr. and Meth. A **494** (2002) 402.
[15] J.E. Gaiser, Ph.D. thesis, SLAC-R-255 (1982).
[16] CLEO Collaboration, A. Anastassov et al., Phys. Rev. Lett. **86** (2001) 4467.
[17] For instance, for the $K^-\pi^0\eta\nu_\tau$ measurement the cross-feed from $\pi^-\pi^0\eta\nu_\tau$ decay was not considered, although it gives the largest contribution as seen in Table I.